Mem. S.A.It. Vol. 90, 374

Memorie della

Properties of single-line spectroscopic binaries detected in the Gaia-ESO Survey

T. Merle[1], M. Van der Swaelmen[2], S. Van Eck[1], and A. Jorissen[1]

[1] Institut d'Astronomie et d'Astrophysique, Université Libre de Bruxelles, CP. 226, Boulevard du Triomphe, 1050 Brussels, Belgium, e-mail: tmerle@ulb.ac.be
[2] INAF - Osservatorio Astrofisico di Arcetri, Largo E. Fermi 5, 50125 Firenze, Italy

Abstract. The *Gaia*-ESO Survey (GES) has allowed to detect several hundreds of spectroscopic binaries with one visible component (SB1) among 43400 stars in the internal Data Release 5. A statistical χ^2 test is applied on the radial velocity (RV) time series to identify RV variables. The main cause of the RV variability is not only the binarity but also stellar pulsations and jitter due to atmospheric convection. To identify SB1 among the RV variables, we defined a criterion based on the intrinsic GES RV dispersion and the intrinsic photometric dispersion using *Gaia* DR2 photometry. After correction for the detection efficiency, we estimate the SB1 fraction to about 10%. Using the GES recommended parameters, we investigated the dependence of the SB1 fraction with the effective temperature and metallicity. The SB1 fraction decreases with metallicity at a rate of $-9 \pm 3\%$ dex^{-1} on the metallicity range $-2.5 \leq$ [Fe/H] $\leq +0.5$. This anti-correlation is established for the first time on a large metallicity range and for a homogeneous sample. This decrease with metallicity seems, within the error bars, independent of the spectral type and the evolutionary stage.

Key words. binaries: close – binaries: spectroscopic – techniques: radial velocities

1. Introduction

The properties of binary stars are fundamental to understand how they were formed and how they evolve. Interaction processes between components may lead to complex outcomes observed in stellar families like Ba, CH, CEMP, etc. stars. We report the detection and characterisation of spectroscopic binaries with one visible component in the *Gaia*-ESO Survey (GES) internal Data Release 5.

The GES is a ground-based multi-object spectroscopic survey targeting one hundred thousand stars with the goal to study the formation and evolution of stellar populations of the Milky Way using kinematical and chemical characterisation (Gilmore et al. 2012; Randich et al. 2013). This survey is not designed to monitor variable or binary stars. Nevertheless, it was already possible to detect hundreds of SB2, tens of SB3 and even one SB4 candidate Merle et al. (2017) using an automated technique to identify multi-peak cross-correlation functions on single exposures (Van der Swaelmen et al. 2017, 2018a,b). Because 4 single exposures per target are generally available, it is also possible to search for SB1 systems (Merle et al. 2018).

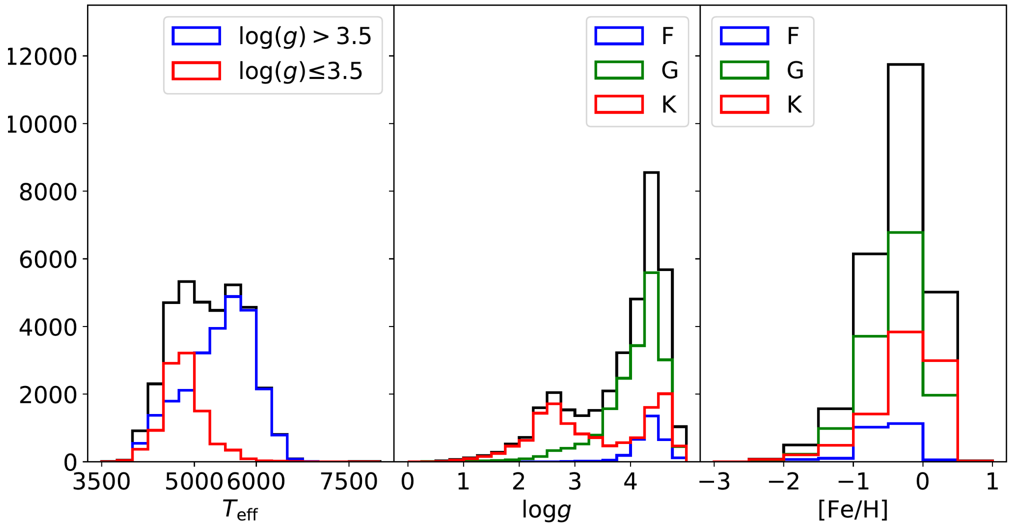

Fig. 1. Distribution of the GES iDR5 recommended atmospheric parameters for the analysed stellar sample. Black distributions are the sum of coloured ones. The $T_{\rm eff}$, $\log g$ and [Fe/H] bin size are 250 K, 0.25 and 0.5 dex, respectively.

2. Properties of the stars observed in the GES

The analysed sample is made of FGK main sequence (MS), turn-off (TO) and red giant branch (RGB) stars. We represent the distribution of the GES stars in terms of effective temperature, surface gravity and metallicity (Fig. 1). To explain the shape of the black distributions we separate them as a function of $\log g$ or spectral type.

The distribution of effective temperatures (left panel of Fig. 1) shows two peaks: one at 5000 K (K spectral type) and one at 5750 K (G spectral type). The peak corresponding to the G spectral type is mainly due to MS and TO stars, whereas the peak corresponding to the K spectral type is mainly due to giant stars. The distribution in surface gravity indeed shows that F-type stars are on the MS, G-type star are found from MS to RGB through TO, and K spectral-type show clearly two populations: one on the MS and one on the RGB. The metallicity distribution of each spectral types cover the whole metallicity range ($-3 <$ [Fe/H] < 1).

The spectra are mainly obtained using the medium resolution GIRAFFE/FLAMES spectrograph (Pasquini et al. 2002) with HR10 ([5340, 5610] Å, $R \sim 21\,500$) and HR21 ([8490, 9000] Å, $R \sim 18\,000$[1]) gratings. The HR21 region includes the Paschen lines and the Ca II near IR triplet, which is observed by the RVS spectrograph of the *Gaia* space mission.

The median magnitude of the GES sources for the analysed sample is 15.4, the median signal-to-noise ratio (S/N) of single exposures is about 14.6 when considering HR10 and HR21 gratings. Most important for the study of SB1 is the number of exposures per target which is about 4: generally 2 consecutive exposures with HR10 and 2 with HR21, but the number can vary, from 2 exposures to tens. The distribution of the maximum time span per target shows that the time sampling is irregular: from half an hour to the duration of the survey (5 years).

[1] For measurements taken before 2015-02-02, the resolving powers are 19 800 and 16 200 for HR10 and HR21 respectively.

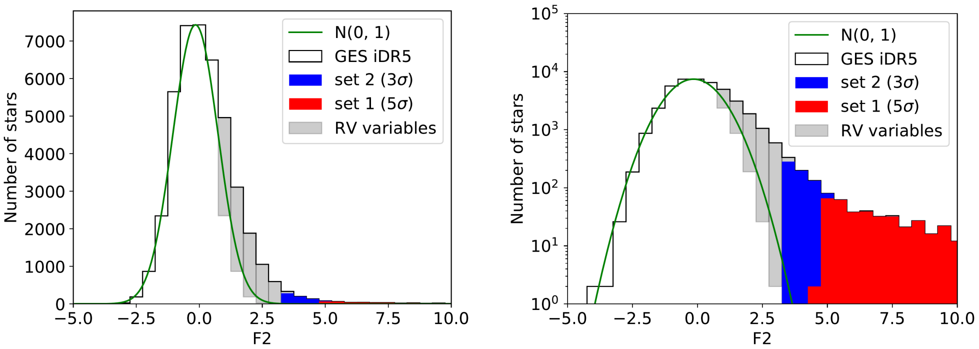

Fig. 2. F2 distribution of the analysed sample. The right tail of the distribution shows all RV variables (grey area), as well as 3σ (in blue) and 5σ (in red) confidence levels. Left: linear scale. Right: logarithmic scale.

3. The statistical χ^2 test to detect RV variables

We use three different criteria to define our sub-sample of GES stars:

- $S/N \geq 3$: we consider only RV measurements from exposures with sufficient signal-to-noise ratio;
- $\Delta v_{\rm max} < 140$ km s^{-1}: multiple exposures that show RV differences larger than this value are discarded;
- $\Delta v/\Delta t < 62.5$ (km s^{-1})/h: we reject targets that show nonphysical acceleration.

The detailed justification of these values are explained in Merle et al. (2020). These criteria lead to a stellar sample of 43400 FGK stars.

We apply a statistical χ^2-test of the RV time series derived by Van der Swaelmen et al. (in prep.) for each star, taking care to estimate properly the uncertainties. The RV measurements from HR21 grating are corrected for the inter-setup bias (0.5 km s^{-1}). For each RV measurement, the resulting attached uncertainty is the square root of the quadratic sum of the Gaussian fit error, the physical error and the spectrograph configuration error. The Gaussian fit error is generally negligible (about 0.03 km s^{-1}); the physical error (Van der Swaelmen et al., in prep) includes the effect of effective temperature (and to a lower extent, the gravity and metallicity) and the effect of the S/N (typical value of about 0.5 ± 0.3 km s^{-1}); finally, the spectrograph configuration error (0.2 and 0.3 km s^{-1} for HR10 and HR21 respectively) is due to changes in the wavelength calibration with time and changes in fibre allocation.

Because the number of observations per star is not constant, we cannot directly compare χ^2 of different objects. We need the $F2$ statistics that makes χ^2 independent of the degree of freedom and transform the asymmetric distribution of χ^2 to a symmetric standard normal distribution $\mathcal{N}(0, 1)$. Then, the $F2$ distribution of a population of single stars with variable number of exposures should follow the standard normal distribution. The $F2$ distribution is displayed on Fig. 2. The distribution of observed $F2$ is centred on zero meaning that uncertainties are well estimated, but is not symmetric, which is the sign of the presence of a population of RV variables. When we compare with the standard normal distribution (in green) we see that the left side is well reproduced, but the right side shows an extended tail toward large $F2$ values. This excess of RV variables is shown in grey and represents 22% of the sample. Nevertheless, they cannot be identified. To be very conservative, we consider a first set of RV variables at 5σ (set 1, in red in Fig. 2), and a second set a 3σ (set 2, in blue).

4. Selection of SB1 from RV variables

This excess of 22% of RV variables can be ascribed to binarity but also to single stars show-

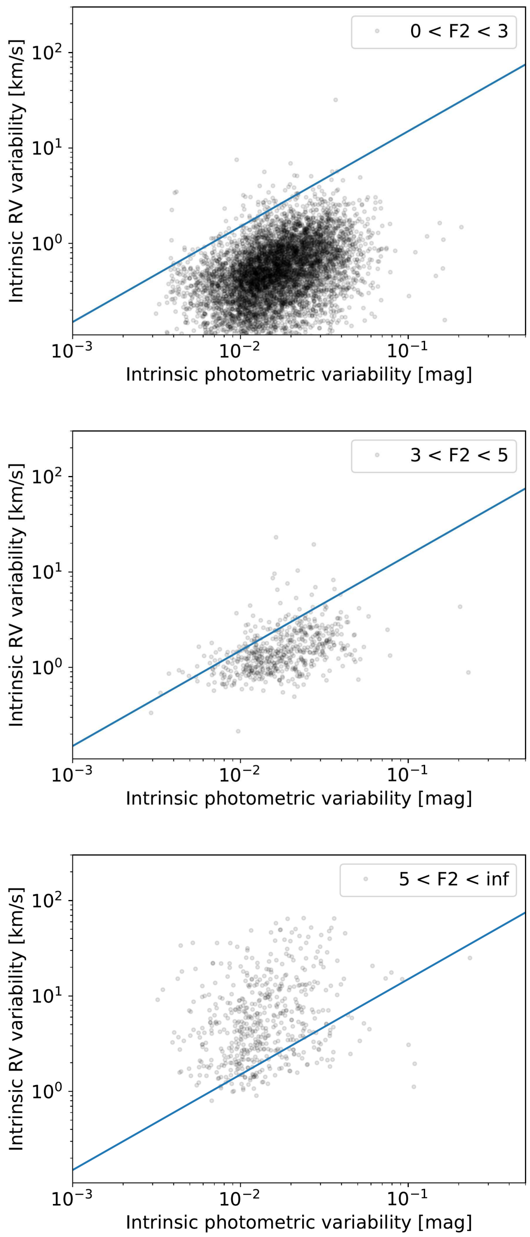

Fig. 3. Intrinsic RV variability as a function of intrinsic photometric variability for dwarf stars. Blue line represents a criterion to avoid δ Sct whose pulsations induced RV variations. Stars above this line are considered as SB1. Top: stars with $F2$ between 0 and 3 that mainly consist in single stars. Middle: stars with $F2$ between 3 and 5 with fraction above the blue line being SB1. Bottom: stars with $F2$ above 5 that are mainly SB1.

ing photometric variations like pulsations or jitter or having spots on their surfaces. Let's explain how we proceed to remove photometric variables. We cross-matched GES targets with *Gaia* DR2 (*Gaia* Collaboration 2018) to obtain the colour-magnitude diagram of GES stars, and designed a luminosity criterion to discriminate between dwarfs and giants because the sources of photometric variability are different in nature for stars on the main sequence and for giant stars. In the analysed FGK stellar sample, photometric variability of dwarfs is represented by δ Sct F-type stars while variability in giants mainly comes from pulsation of stellar envelopes and to a lower extent to the presence of spots on the stellar surfaces.

We compared the intrinsic RV dispersion coming from the RV measurements of the GES spectra as a function of the intrinsic photometric dispersion of the *Gaia G* band (Fig. 3). In single star populations, RV dispersion due to pulsations is expected to linearly increase with the photometric dispersion. This means that a high intrinsic RV dispersion do not warrant the star to be a SB1 especially if the associated intrinsic photometric dispersion is high. In particular for δ Sct stars, Breger et al. (1976) shows that the ratio between the full RV amplitude and the V-band photometric variations ranges from 50 to 125 km s^{-1} mag^{-1}. To discriminate δ Sct regime from the one of spectroscopic binarity, we use a conservative threshold of 150 km s^{-1} mag^{-1}, displayed as a blue line on the plots of Fig. 3. To emphasise how we can extract SB1 from RV variables, we represent the intrinsic RV dispersion vs. the photometric one by range of $F2$. For $F2 < 3$ (top panel), most of stars, including 19% of stars that are RV variables, falls below the threshold and are believed to be single stars. For $3 < F2 < 5$ (middle panel), stars are RV variables, represent 1.5% of the whole FGK analysed sample and most of them are not SB1 because falling below the threshold. For $F2 > 5$ (bottom panel), most stars are above the threshold and believed to be all SB1.

For giant stars, we use a similar linear threshold to discriminate SB1 from RV variables due to low-amplitude envelope pulsations (Kjeldsen et al. 1995) as performed by Jorissen et al. (1997). We have a similar behaviour from low to high value of $F2$, excepted that less RV variables fall below the threshold when $3 < F2 < 5$.

If we consider the 3% of RV variables defined by set 2, we obtain, after removal of photometric variables, 520 SB1 dwarfs, 200 SB1 giants (and 85 without classification), that represents a raw SB1 rate of 2% of the analysed FGK sample. The detection efficiency is dominated by the GES time baseline, which has not been designed to maximise binary star detection. By taking into account the GES detection efficiency (see Merle et al. 2020), we obtain a corrected SB1 fraction of about 10%.

5. SB1 distribution and fraction with effective temperature

We display the number distributions of GES and SB1 stars as well as the corrected SB1 fractions as a function of the FGK spectral type on Fig. 4, for dwarf stars on the left panels and for giant on the right panels. The distributions are set on logarithmic scale to see the SB1 distributions as they represent only a few percents of the analysed sample. The SB1 samples follow the distribution of the analysed sample, peaking at spectral type G for dwarfs and spectral type K for giants. The distribution of SB1 is independent of the adopted confidence level (set 1 or 2).

When we take into account the detection efficiency, we obtain the corrected SB1 fractions for set 1 (red) and 2 (blue), as shown on bottom panels of Fig. 4. For SB1 with dwarf primaries, we obtain an increase with the increasing temperature from K to F spectral types, in agreement with previous studies. For SB1 with giant primaries, we obtain a larger fraction for K spectral type, but the large errors bars prevent us from drawing any firm conclusion. This could be due to an underestimation of the detection efficiency for SB1 with giant primaries of spectral type K. The comparison with literature is only feasible for SB1 with dwarf primaries. We compared our results with Clark et al. (2012); Duchêne & Krauss (2013); Gao et al. (2014); Moe & Di Stefano (2017), and found similar increase of the SB1 frac-

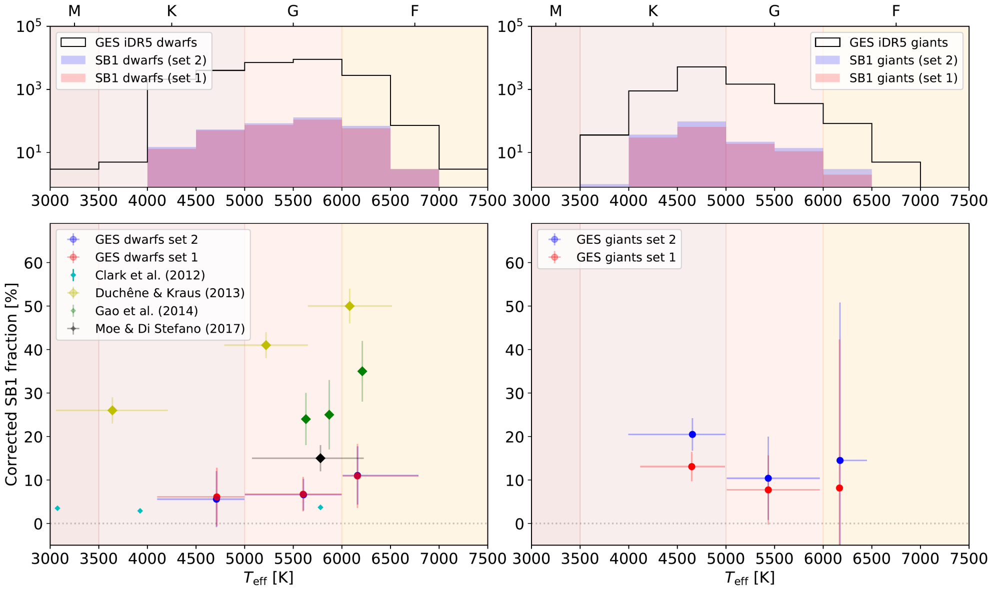

Fig. 4. Top panels: number distribution of GES stars and detected SB1 with effective temperature. Bottom panels: corrected SB1 fraction with effective temperature for dwarfs (left panel) and giants (right panel). Red and blue colours correspond to sets 1 and 2. The dots are centred on the median $T_{\rm eff}$ in each spectral type and the $T_{\rm eff}$ range in each spectral type is illustrated by the horizontal error bars.

tion with effective temperature. Nevertheless, our slope is less pronounced. The large values of Duchêne & Krauss (2013) are related to the fact that their binary fraction included long-period binary systems detected by other techniques.

6. SB1 distribution and fraction with metallicity

We displayed the number distributions of GES and SB1 stars as well as the corrected SB1 fraction as a function of metallicity on Fig. 5. Due to the low number of SB1 with derived metallicity, we combined SB1 with dwarf and giant primaries to have statistically significant fractions in each bin of metallicity in the range $[-2.5, 0.5]$. The number distribution of SB1 follows the one of the analysed sample that peaks at [Fe/H]$= -0.5$.

When we take into account the detection efficiency, we obtain the corrected SB1 fraction for set 1 (red) and 2 (blue), as shown on bottom panel of Fig. 5. Both sets show a clear anti-correlation with metallicity. A linear fit of the corrected SB1 fraction with metallicity provides a slope of $-9 \pm 3\%$ dex^{-1} and a y-intercept of $8 \pm 2\%$. These results are in a good agreement with Grether & Lineweaver (2007) who study FGK binaries within 25 pc (with a maximum 5 y period systems). We note that our SB1s can reach 10 kpc. They do not find such anti-correlation in their extended sample that reaches 50 pc. Gao et al. (2014) obtained very large binary fractions but their analysis are based on low resolution SDSS data. Finally, in a recent study on APOGEE data, Badenes et al. (2018) provide the ratio between low ([Fe/H] $= -0.3$) and high ([Fe/H] $= +0.1$) metallicity binaries. Assuming a value for high metallicity fraction (8%) we found a similar trend with our.

In a recent meta analysis, Moe et al. (2019) combined different spectroscopic surveys that they corrected for completeness and various biases and got a trend with two distinct slopes (see their figure 18). The trend derived in the present paper is located on the lower part of

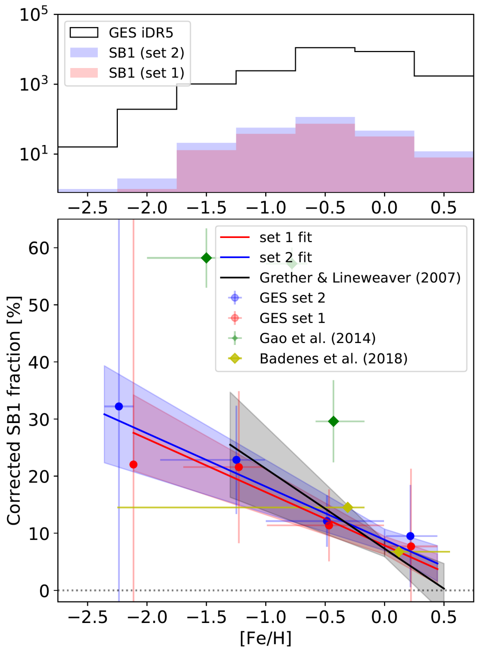

Fig. 5. Top panel: number distribution of GES stars and detected SB1 with metallicity. Bottom panel: corrected SB1 fraction with metallicity. Red and blue colours correspond to sets 1 and 2. The dots are centred on the median metallicity in each bin of 1 dex, and the metallicity range in each bin is illustrated by the horizontal error bars.

their error bars. The strength of our study relies on the homogeneous analysis of the GES data over a wide range of metallicities.

We also show in more details in Merle et al. (2020) that the metallicity dependence in the range [$-2.5, 0.5$] of the corrected SB1 fraction seems to be independent of the spectral type (FGK) and the evolutionary stage (MS/RGB) within the error bars.

7. Conclusions

We present the detection and characterisation of SB1 using single exposures from the GIRAFFE HR10 and HR21 gratings. We apply a statistical χ^2-test on a sample of 43400 FGK stars that were observed at least twice and have $S/N \geq 3$, $\Delta v_{\max} < 140$ km s^{-1}and $\Delta v/\Delta t < 62.5$ (km s^{-1})/h. This χ^2-test allows to identify RV variables. However, this sample consists both in SB1 and in stars with photometric variability that induces RV variations. We use the *Gaia* DR2 parallaxes and photometry to discriminate MS and RGB stars because the origin of the photometric variability differs in nature for dwarf and giant stars. By applying criteria in the intrinsic RV vs. G band photometry dispersion plane, we select the SB1 candidates from the RV variables. We end up with 800 SB1 candidates at 3σ confidence level. This number is reduced to 640 if the confidence level is increased at 5σ. The corrected SB1 fraction increases with the effective temperature for SB1 with dwarf primaries while this conclusion is unclear for SB1 with giants. We establish that the corrected SB1 fraction increased with decreasing metallicity at a rate of -9 ± 3% for the metallicity range [-2.5, 0.5] with a value of 8 ± 2 at solar metallicity. We investigated in more details the dependence of the corrected SB1 fraction as a function of the spectral type (FGK) and the evolutionary stage (MS/RGB) in Merle et al. (2020).

Acknowledgements. T.M. and S.V.E. are supported by a grant from the Fondation ULB.

References

Badenes, C., Mazzola, C., Thompson, T. A., et al. 2018, ApJ, 854, 147
Breger, M., Hutchins, J. & Kuhi, L. V. 1976, ApJ, 210, 163
Clark, B. M., Blake, C. H. & Knapp, G. R. 2012, ApJ, 744, 119
Duchêne, G., & Krauss, A. 2013, ARA&A, 51, 269
Gaia Collaboration, Brown, A. G. A., Vallenari, A., Prusti, T., et al. 2018, A&A, 616, A1
Gao, S., Liu, C., Zhang, X., et al. 2014, ApJ, 788, L37
Gilmore, G., Randich, S., Asplund, M., et al. 2012, The Messenger, 147, 25
Grether, D. & Lineweaver, C. H. 2007, ApJ, 669, 1220
Jorissen, A., et al. 1997, A&A, 324, 578
Kjeldsen, H., et al. 1995, AJ, 109, 1313
Merle, T., Van Eck, S., Jorissen, A. et al. 2017, A&A, 608, A95

Merle, T., Van der Swaelmen, M., Van Eck, S., et al. 2018, SF2A-2018: Proceedings of the Annual meeting of the French Society of Astronomy and Astrophysics, eds. P. Di Matteo, et al., 107
Merle, Van der Swaelmen, Van Eck et al., 2020, A&A, 635, A155
Moe, M. & Di Stefano, R., 2017, ApJS, 230, 15
Moe, M., Kratter, K. M., Badenes, C. 2019, ApJ, 875, 61
Pasquini, L., Avila, G., Blecha, A., et al. 2002, The Messenger, 110, 1
Randich, S., Gilmore, G. & *Gaia*-ESO Consortium, 2013, The Messenger, 154, 47
Van der Swaelmen, M., Merle, T., Van Eck, S. et al. 2017, in SF2A-2017: Proceedings of the Annual meeting of the French Society of Astronomy and Astrophysics, eds. C. Reylé, et al., 307
Van der Swaelmen, M., et al. 2018, SF2A-2018: Proceedings of the Annual meeting of the French Society of Astronomy and Astrophysics, eds. P. Di Matteo, et al., 183
Van der Swaelmen, M., Merle, T., Van Eck, S. et al. 2018, IAU Symposium, 330, 183